Institute of Paper Science and Technology
Atlanta, Georgia

IPST Technical Paper Series Number 661

High-Speed Infrared Detection of Coated Roll Surface Defects

C.S. Korach, T.F. Patterson, and D.I. Orloff

June 1997

Submitted to
1997 TAPPI Engineering & Papermakers Conference
Nashville, Tennessee
October 6–9, 1997

INSTITUTE OF PAPER SCIENCE AND TECHNOLOGY
PURPOSE AND MISSIONS

The Institute of Paper Science and Technology is a unique organization whose charitable, educational, and scientific purpose evolves from the singular relationship between the Institute and the pulp and paper industry which has existed since 1929. The purpose of the Institute is fulfilled through three missions, which are:

- to provide high quality students with a multidisciplinary graduate educational experience which is of the highest standard of excellence recognized by the national academic community and which enables them to perform to their maximum potential in a society with a technological base; and

- to sustain an international position of leadership in dynamic scientific research which is participated in by both students and faculty and which is focused on areas of significance to the pulp and paper industry; and

- to contribute to the economic and technical well-being of the nation through innovative educational, informational, and technical services.

ACCREDITATION

The Institute of Paper Science and Technology is accredited by the Commission on Colleges of the Southern Association of Colleges and Schools to award the Master of Science and Doctor of Philosophy degrees.

NOTICE AND DISCLAIMER

The Institute of Paper Science and Technology (IPST) has provided a high standard of professional service and has put forth its best efforts within the time and funds available for this project. The information and conclusions are advisory and are intended only for internal use by any company who may receive this report. Each company must decide for itself the best approach to solving any problems it may have and how, or whether, this reported information should be considered in its approach.

IPST does not recommend particular products, procedures, materials, or service. These are included only in the interest of completeness within a laboratory context and budgetary constraint. Actual products, procedures, materials, and services used may differ and are peculiar to the operations of each company.

In no event shall IPST or its employees and agents have any obligation or liability for damages including, but not limited to, consequential damages arising out of or in connection with any company's use of or inability to use the reported information. IPST provides no warranty or guaranty of results.

HIGH-SPEED INFRARED DETECTION OF COATED ROLL SURFACE DEFECTS

C. S. Korach
Technician
IPST
Atlanta, GA 30318
USA

T. F. Patterson
Senior Associate Engineer
IPST
Atlanta, GA 30318
USA

D. I. Orloff
Professor of Engineering
IPST
Atlanta, GA 30318
USA

ABSTRACT

Cermet roll coatings have become an important component of paper machine press rolls with the increased use of cermet coatings as granite roll substitutes and recent developments in impulse drying. Given these developments, one would like to know how well cermet coatings withstand thermal and mechanical cyclic loading over an extended period of time. Using infrared thermography techniques, it should be possible to determine when and how the cermet coatings fail; coating failures are detected by temperature differentials between a defect and the surrounding coating. To establish how well the infrared thermography can detect various defects in a cermet coating, a study was conducted using a high-speed, high-resolution infrared thermal imaging and data acquisition system. A press roll rotating at 328 RPM (628 m/min, 2061 fpm), with coating defects of various shapes and sizes, was imaged. The defects were classified as either circular or line defects based on their shape and method of forming. Resolution of 2.38 mm (3/32") was achieved with the circular defects and a resolution of 1.59 mm (2/32") with the line defects. The dimensional accuracy of the method was also quantified. The successful identification of these defects supports the implementation of infrared imaging as a viable method of identifying coating failures at high roll speeds.

INTRODUCTION

Coated surfaces have been recognized as an integral factor in preventing delamination in impulse drying of linerboard.[1-3] Coatings that possess low conductivity, low density, and low specific heat control energy transfer to the sheet, thus reducing flash evaporation inside the sheet during nip depressurization. Ceramics and some cermets have these properties. Initially, machinable ceramics were tested with impulse drying, but recent developments have led to the use of plasma-sprayed ceramics and cermets. Plasma-spraying reduced the cost of ceramic roll coatings and made possible the use of cermet roll coatings.

This work is part of a larger study to determine the long-term durability of plasma spray coatings in the impulse drying application environment. As a first step in that work, a method for detecting roll coating defects while the roll is moving was in need of development. This paper discusses the experimental apparatus that was built to conduct the roll surface durability study and the methods to be used in detecting roll defects as they may develop with time.

Infrared detection of material defects is a commonly used NDE (Non Destructive Evaluation) method.[4-10] A number of researchers have developed experimental techniques for detecting defects in coated materials using IR NDE. Connolly investigated detection of subsurface defects in various coating/substrate combinations, including ceramic/metal, metal/metal, and ceramic/ceramic structures.[5] McKnight and Martin developed a method for detecting defects in organic coatings on steel substrates.[7] Ogura and Sakagami investigated defects in metal plates with attention given to the differences between defects oriented perpendicular to the plate and parallel to the plate.[6] Satonaka et al. performed a similar study, which concentrated on defects in welds.[8] All of these studies involved stationary objects. In addition, all the measurements were made using transient heating of the objects. The object was initially at ambient conditions; it was then heated for a short period of time (several milliseconds to several seconds). The infrared measurements were taken during that time period.

The study reported in this paper involved detecting small defects in a coated roll continuously maintained at an elevated temperature and rotating at more than 300 RPM. The only similar study reported in the literature was by Lahdeniemi et al.[9] That study reports on IR temperature measurements of paper-machine felts moving at 600-1200 m/min.

The coating failures are hypothesized to develop in either of two forms:

1. A surface defect, where the bond between a section of coating and the substrate has failed and the section of coating is removed, creating an area of reduced coating thickness or exposing the metal surface below.

2. A subsurface defect, where the bond between a section of coating and the substrate has failed, but the coating remains on the object, creating an air-filled blister-type structure.

In this experimental setup, the induction heater produces eddy currents in the steel shell of the roll causing the shell to heat

1

due to Joule heating. Thus, the first type of defect would appear as a hot spot because the ceramic coating around the defect would act as a thermal insulator. This was observed, although there were some unexpected temperature profiles also observed. These showed a temperature decrease at the defect edge. A possible explanation for this was variations in convective heat loss. This was investigated using a 2-D FEM.[12] Results demonstrated that variations in convection coefficients, possibly caused by turbulence at the defect edge, could create this type of temperature profile.

The second type of defect would appear as a cold spot because the air has a low thermal conductivity.[7] This type of defect was not investigated.

BACKGROUND - Using Infrared Thermography to View Coating Failures

As discussed previously, IR thermography is a widely used NDE tool for detecting surface and subsurface flaws in coated materials. IR detectors look at the intensity of photon radiation emitted by an object. In theory, the blackbody radiation intensity is governed by Planck's law, which varies with wavelength and temperature:

$$I_{\lambda,b}(\lambda, T) = \frac{2hc_o^2}{\lambda^5 \left[\exp(hc_o / \lambda kT) - 1 \right]} \qquad (1)$$

Where λ is the wavelength; T is the absolute temperature of the blackbody; h is Planck's constant; c_o is the speed of light in a vacuum; and k is the Boltzmann constant.[11] The IR scanner used in this study is a short wavelength scanner and only detects photon radiation with wavelengths in the 2 to 5.4 μm range utilizing a limited solid angle.[7] This allows temperature to be the only variable.

The objects imaged in this study are greybodies and not blackbody emitters. The spectral properties of the object consist of the absorptivity (α), emissivity (ε), reflectivity (ρ), and the transmittance (τ). These factors all must be taken into consideration when determining the temperature of a gray object. Assuming the coatings are opaque, then the transmittance (τ) of radiation through the object is equal to 0. From blackbody theory, the sum of the absorptivity (α) and reflectivity (ρ) must equal 1. Kirchoff's law states: $\varepsilon = \alpha$; therefore, the object reflectivity can be determined from the emissivity. The AGEMA 900 system allows the object emissivity to be specified. The system also compensates for transmission through the atmosphere.[7, 10-11]

For this study, only relative temperatures were of importance, but it was attempted to record temperatures as accurately as

possible. Therefore, the emissivity of the coating surface was estimated to be 0.86 from the known emissivity of other like ceramic coatings. The atmospheric transmittance was calculated using an AGEMA algorithm.

EQUIPMENT

Roll/Machine

Figure 1 shows the apparatus. The primary components of the apparatus consisted of a single nip roll press, an induction heater used to heat the upper press roll, a high-speed, high-resolution thermal imaging system, and a continuous wet felt, which passes through the press nip. The lower (unheated) roll had a 12.7 mm (0.5 in) thick polyurethane coating. The upper (heated) roll had a three-layer plasma-sprayed coating. The base layer, applied directly to the steel roll, was a metal alloy bond coat. The middle and thickest layer was a partially stabilized zirconia (PSZ) coat. The top, or outside, layer was a dense (reduced void volume) PSZ coat. The combined thickness was approximately 0.762 mm (0.030 in). The top coating was diamond ground to a 1.01 μm R_a finish.[1] The ceramic-coated roll was heated to 200°C (392°F) by the induction heating system. The induction heater produced electromagnetic eddy currents within the steel shell of the roll, resulting in heating of the shell. The heat was transferred from the steel to the thin ceramic coating by conduction. The roll constantly rotated beneath the induction heating coils, giving constant and even heating. The roll temperature (200°C) was chosen because it is comparable to the temperature at which an impulse dryer press would operate. The peak nip pressure was 6.9 MPa (1000 psi). A wet felt was passed between the two rolls to quench the heated roll and hence to create a cyclic thermal and mechanical loading on the coating. The rolls rotated at 328 RPM, which translated to 628 m/min (2061 fpm) based on the 0.61 m (2 ft) roll diameter. This speed was comparable to conventional linerboard machine speeds.
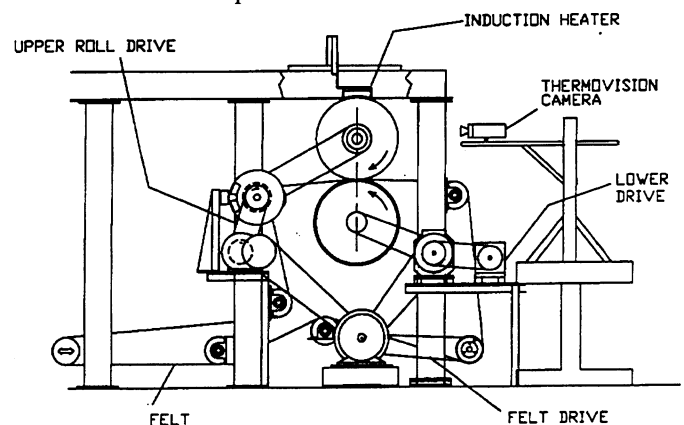

Fig. 1 Roll Coating Durability Test Stand, back side view.

Defects

The defects were placed on the drive side of the roll in the machine direction. Forty-five defects, varying in shape, size, and depth, were made in the roll coating. The coating defects were produced using standard drill bits and milling machine bits for the circular defects and grinding wheels of a variety of thicknesses for the straight line patterned defects.

There were a total of 37 circular defects, 24 that were made with standard drill bits. The bit sizes were: 0.79, 1.19, 1.59, 2.38, 3.18, 3.97, 4.76, and 5.56 mm (1/32, 3/64, 2/32, 3/32, 4/32, 5/32, 6/32, and 7/32 of an inch). The holes were placed in rows of three holes for each defect size, making a total of 8 rows. Three holes were used for each size defect to increase the number of data points. This also made possible a study of variability across the roll in the cross machine direction. Depths of the defects were dependent on the bit diameter, the center of the defect extended through the coating to the base metal on most drill defects. The remaining 15 circular defects were made using milling bits. Milling bits were used on the larger defects because as the drill bit diameter increased the tip camber also increased. The larger drill bits would produce an excessively deep defect, one that extended significantly into the base metal. The mill bits have a flat tip, which allows for a shallow defect with a uniform depth. The mill bit sizes used were: 3.97, 4.76, 6.35, 7.94, and 9.53 mm (5/32, 6/32, 8/32, 10/32, and 12/32 of an inch). The defects varied in actual sizes from the specified mill bit size due to cracking of the ceramic around the edges of the defect.

Seven of the remaining defects were comprised of different length, width, and depth lines. The line defects were made using a grinding wheel. Depth was determined by visually inspecting the defect to see whether the surface of the coating had been partially penetrated or if the defect extended to the steel roll surface. The thickness of the line defects ranged from 0.40 to 3.18 mm (1/64 to 4/32 of an inch). Three defects were made to demonstrate the distinction between defects of the same shape, but with increasing thicknesses of: 0.79, 1.59, and 3.18 mm (1/32, 2/32, and 4/32 of an inch). Another set of two defects was made to highlight the effect of varying thicknesses and lengths of line defects in the horizontal and vertical directions. These defects were more complex comprising of at least five lines per defect. A set of two defects was made in the pattern of a diagonal cross to study the effect of imaging diagonal lines on the roll surface. These defects were made with varying depths (scraped to the bare steel or not to the bare steel) and different thicknesses: 0.40, 0.79, and 1.59 mm (1/64, 1/32, and 2/32 of an inch). The final line defect was made by scratching the surface of the ceramic coating.

Scanner/Data Taking

An AGEMA 900SW/TE thermal imaging system was used to acquire all the data. The system is a high-speed, high-resolution thermography tool. It is comprised of a thermo-electrically cooled IR scanner, a high-speed system controller with a 1 Gb hard disk and a 32 Mb ramburst for high-speed data acquisition, a high-resolution video monitor, and an external 1.3 Gb optical disk drive for data backup and storage. The scanner was provided with a 40-degree FOV IR lens. The scanner has the capability of scanning at a rate of either 20 or 30 Hz. It also has the capability of linescanning at a rate of 3.5 kHz.

The scanner focal plane was positioned approximately 10 cm (4 in) from the roll surface. Given the 40-degree FOV lens, the resulting image encompassed only the section of the roll containing the defects. The scanner imaged the roll through a PFA Teflon window (thickness = 2.29 mm (0.090 in)), which was fixed to a stainless steel internally cooled enclosure to prevent the scanner from being damaged by the high temperatures and the extreme humidity. The enclosure was cooled using a compressed air vortex cooler in conjunction with a thermocouple probe monitoring the temperature. The PFA Teflon window attenuated the IR transmittance to the scanner. The transmittance through this particular IR window was determined to be $\tau = 0.26$. The transmittance was calculated using the AGEMA option of inputting an estimated transmittance value into the temperature calculation algorithm and matching the calculated temperature with a thermocouple probe temperature on the coating surface. This transmittance was input into the temperature calculation algorithm to compensate for the attenuation.

Data were taken at a rate of 3.5 kHz over a 10-second period and recorded directly to the ramburst drive. The data were taken while the scanner was in linescanning mode. The thermal imaging system has the ability to create a single high-resolution image from a linescan file of multiple cyclic images that are triggered at each cycle. It accomplishes this by comparing all of the synchronized cyclic images and interlacing lines from different images together to form a more detailed image. To synchronize the linescan with the roll rotation, a magnetic pickup was added to the top roll shaft of the machine to trigger the system every roll revolution. The computer then compiled 40 revolutions of data into a complete high-resolution line sequence of one roll revolution that contained 3227 lines.

RESULTS

Results were analyzed using the AGEMA Erika software, Microsoft Excel for data analysis and 3-D surface plots, and Harvard ChartXL for 2-D contour plots. The AGEMA

software was setup to dump an image file into an ASCII format file that can then be imported into DOS. The file format was setup in the form of a 2-D pixel array with the individual array element values corresponding to the temperature associated with the pixel.

Each defect was measured by a 1/64 inch scale (error = ±1/128 in.) on the roll surface to find the actual dimensions of the defects. The thermal image of the defects was inspected to find the dimension of a single pixel. The AGEMA system has the capability of analyzing images on the pixel level of resolution. To determine the relationship of a pixel to a unit of length, the distance between the centers of the circular defects was measured in the cross machine direction. The true distance between centers was physically measured on the roll surface. This value was divided by the corresponding number of pixels to determine the unit of length to pixel relationship. The AGEMA software was then used to measure the diameters, lengths, and widths of the defects in pixels, which were then converted to a unit of length.

The imaged section of the roll face was 129.5 mm (5.1 in) wide. The image acquired of the defects had an obvious temperature gradient across the roll face. The temperature gradient made possible the comparison of similar defects at different temperatures. The gradient ranged from 163°C (325°F) at the center of the roll face to 193°C (379°F) at the drive side of the roll. The cause of the gradient was due to the felt/roll interaction. Because the felt was only in contact with the center 0.38 m (15 in) of the 0.61 m (24 in) roll width, 0.11 m (4.5 in) on each edge of the roll face was not exposed to the cooling effect of the felt. This created a parabolic temperature profile across the portion of the roll face that was in contact with the felt, with the edges of the felt warmer than the center.

Resolution

The reconstructed images were comprised of 3227 lines (or 3227 pixels in length). This number of lines produced an isomorphic image of the coating (an image that is scaled equally in the vertical and horizontal axis). Based on a roll diameter of 0.61 m (2 ft), the resolution of the image was the circumference (0.61 * π m) divided by 3227. This equated to a resolution of 0.593 mm/line (0.0234 in/line). This resolution corresponds with the value of 0.572 mm/line (0.0225 in/line) calculated from the center-to-center measurements, showing that the resolution around the roll (vertical) was roughly equivalent to the resolution across the roll (horizontal).

Circular Defects

The thermal images of the circular defects had good resolution and well-defined shapes for the larger diameter sizes. The minimum hole diameter identified using the AGEMA thermal

analysis software was 2.38 mm (3/32"). This was determined through the measurement of the pixels that comprise the defects in the thermal image. The drill holes of sizes 1.59 mm (2/32"), 1.19 mm (3/64"), and 0.80 mm (1/32") were not visible with the thermal imaging equipment. These defects apparently were not generating enough of a temperature difference to be visible. The 1.59 mm (2/32") defect was discernible on the 3-D surface plots, but it was very difficult to distinguish between the defect and thermal abnormalities in the coating surface. The 1.19 mm (3/64") and 0.80 mm (1/32") defects were not detectable on the 3-D surface plots. After examination of the thermal data in spreadsheet format, the 1.19 mm defects could be identified.

It is believed that the last three rows of drill defects were difficult to distinguish because of a low temperature difference (ΔT) between the surface of the defect and the surface of the defect surroundings. The maximum defect temperature ($T_{mx,def}$) was low compared with the other defects. After visual inspection of the defects, it was determined that these defects did not penetrate into the steel shell below the cermet. This resulted in the remaining cermet coating acting as an insulator (due to the low thermal conductivity of the cermet), decreasing the $T_{mx,def}$.

It was found that the actual diameter of the circular defects was smaller than the diameter measured using the AGEMA software (Figure 2). It is believed this is due to edge effects. One possible explanation was thermal radiation from the higher temperature bottom of the defect to the lower temperature sides of the defect. An analysis of a cross section of the thermogram showed a ramping of temperature outside and inside the boundary of a defect.

A second possible explanation is variation in convection heat loss across the defect and surrounding area. A 2-D steady-state finite element model of the defect CMD cross section was used to analyze the observed edge effects. Two different cross-sectional geometries were applied to the model:

1. A defect with squared edges and a flat bottom to model the line and mill defects. This geometry utilized a defect bottom with two cases: ceramic and steel.

2. A defect with sloped edges and bottom to model a drill defect. The defect depth was deep enough to expose the steel shell below the ceramic.

Two different boundary condition cases were applied to the geometries, one with a constant heat transfer convection coefficient along the surface and another with a varied convection coefficient.
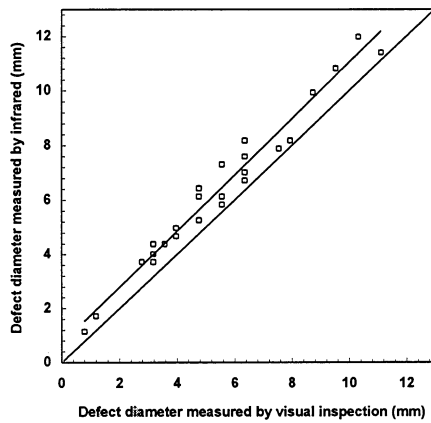
4

Fig. 2 Comparison of defect diameters (mm) by method of detection, infrared scanner versus visual inspection.

Fig. 3 Temperature differentials for circular defects (mill and drill bits).

Fig. 4 Defect temperature differences versus nominal defect diameter (mm).

The model showed that edge effects were generated with the drill defect cross section geometry (i.e., a conical shape) by a varying convection coefficient. This suggests a possible explanation for the edge effect. This same effect was not observed when the model was exercised for square cross-sectional defects such as those in the line defects. This needs to be investigated further.

Cross-sectional analysis of the thermograms also showed that the mill defects plateau at a maximum temperature with gradients on the defect boundaries. The drill defects peak at a maximum temperature and have a sinusoidal shape. It is believed this observation can be explained by the differences in the geometry of the mill and drill defects. The geometry of the mill defects has a flat interior surface with all of the cermet coating removed exposing the steel surface below. The drill defects have sloped sides that extend to a central point below the surface of the roll, the camber of the defects is assumed to be that of the drill bits ~118°. Therefore, the flat surface of the mill defects produces a temperature plateau, and the drill defects produce a peak temperature. Figures 6 and 7 show 2-D finite element models of square cross-sectional defects, similar to the line defects. Figures 8 and 9 show models of conical cross-sectional defects, similar to the circular defects. There is good qualitative agreement with the thermal image data.

Through the use of the 2-D spreadsheet data and the AGEMA software, a comparison between the peak defect temperature and the average of the temperature immediately surrounding the defect was made. This showed that the temperature differential between the defect and its surroundings remained constant along the CD of the roll. Furthermore, because of the presence of a temperature gradient along the CD of the roll face, this analysis showed that defects of similar size, shape, and depth are independent of their surrounding temperature
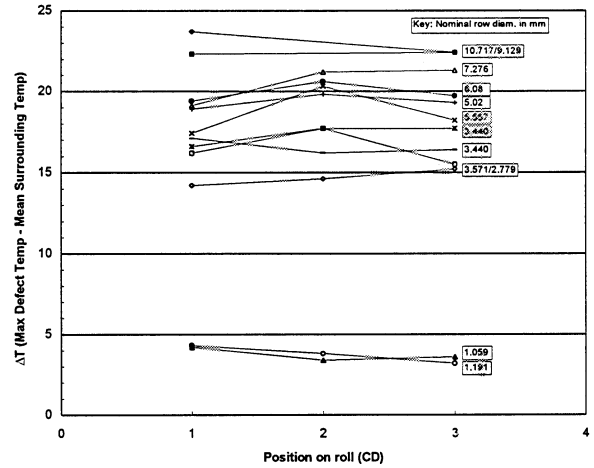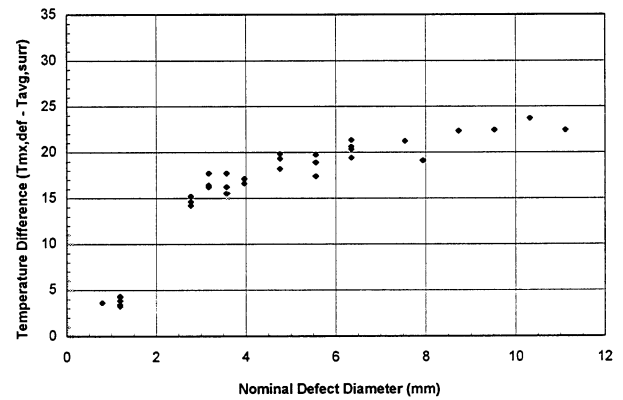
and will consistently show an equal temperature difference (see Figure 3).

It was also observed that as the defect diameter increased the temperature difference between the defect and its surroundings became asymptotic (see Figure 4). The figure shows a sloped set of data, which flatten at the larger diameters (which are mainly mill defects). The smaller defects did not have as large a temperature differential due to the smaller area of exposed steel. The data suggested that once a certain threshold exposed area is exceeded no increases in defect area temperature will be observed.

Line Defects

The line defects proved consistent with the circular defects in as much as the narrowest detectable line width detected with the thermal imaging system was 1.59 mm (2/32"). These images were again analyzed using the AGEMA software, three-dimensional surface plots in Microsoft Excel, and two-dimensional topographical contour plots in Harvard ChartXL.

5

The greater detectability of line defects can be explained by the temperature differential between the defect and the surrounding surface. Infrared scanners determine temperature by detecting the intensity of infrared radiation absorbed by the scanner. Therefore, a larger temperature differential between the defect and the surrounding surface will render the defect more detectable. Circular and line defects with similar widths contained different temperature differentials. The difference is attributed to the shape of the defects; the line defects had square edges, and the circular defects had sloped edges. The defect shape was dependent on the method of defect fabrication, which was previously explained. Using a 3-D surface plot of the defects in Excel, the cross-sectional profile of the 1.59 mm (2/32″) circular and line defects was analyzed. The 1.59 mm (2/32″) line defects were recognizable on the AGEMA system, but the 1.59 mm (2/32″) circular defects were not. It was observed that the circular defect profile contained a smaller temperature gradient at the defect edge (see Figure 5). It is believed the smaller gradient inhibits the maximum defect temperature.

The cross line defects followed a pattern consistent with the other line defects. Each defect was comprised of two lines, each line of a different thickness. The crosses also had lines of different depths, either extending completely to the metal surface or only partially through the cermet coating. A 0.40 mm (1/64″) line did not extend through the cermet. This line was not detected by the AGEMA system. A line of 0.79 mm (1/32″) showed a temperature of less than the temperature of the surrounding environment; this line was deeper than the 0.40 mm (1/64″) line, but did not extend to the metal. The line of 1.59 mm (2/32″) was clearly visible and had an increase in temperature of approximately 4 to 5 degrees centigrade over the surrounding temperature; this line was cut to the metal. It is believed that the 0.40 mm (1/64″) line was not detected because it did not penetrate deep enough into the cermet coating to provide a large enough temperature differential between the defect and the surrounding coating.

The two line defects comprised of vertical and horizontal lines demonstrated similar results. The first defect contained lines of the same thickness, 0.79 mm (1/32″), but one half of the defect had lines cut to the metal, and the other half had defects that were not cut to the metal. The lines that were not cut to the metal shell were detected as having a negative temperature differential with the surrounding coating surface. The opposite was observed with the lines cut to the metal shell; these lines were detected as having a positive temperature differential. The second defect showed a positive temperature differential on every line. The lines were all approximately 1.59 mm (2/32″) thick. Negative temperature differentials were observed on the tips of many of the lines. The line tips ranged from 0.40-0.79 mm (1/64-1/32″) in thickness. Also, the tips of the lines were sloped because of the curvature of
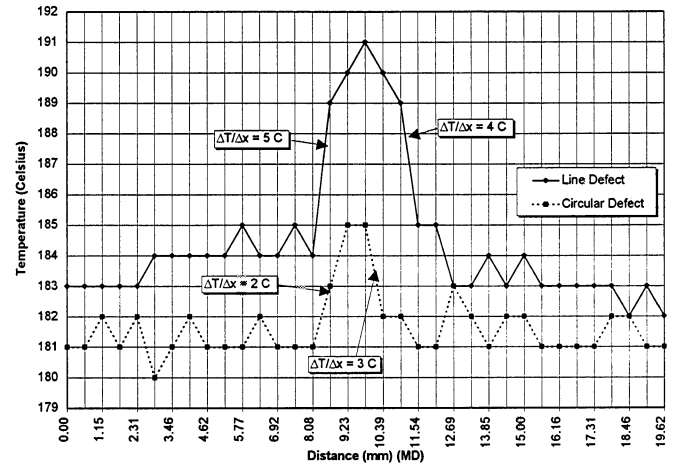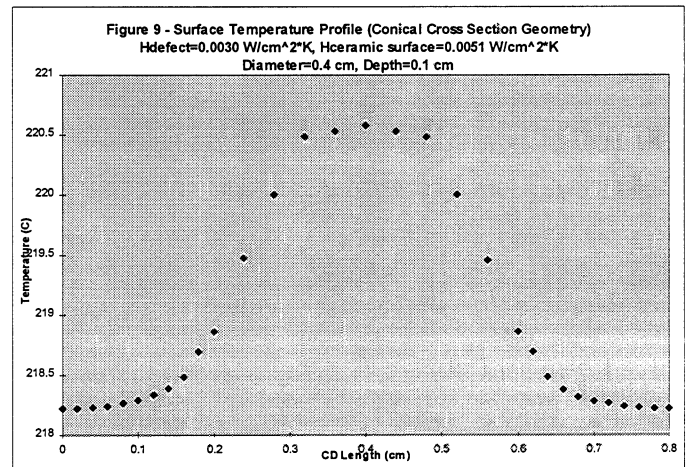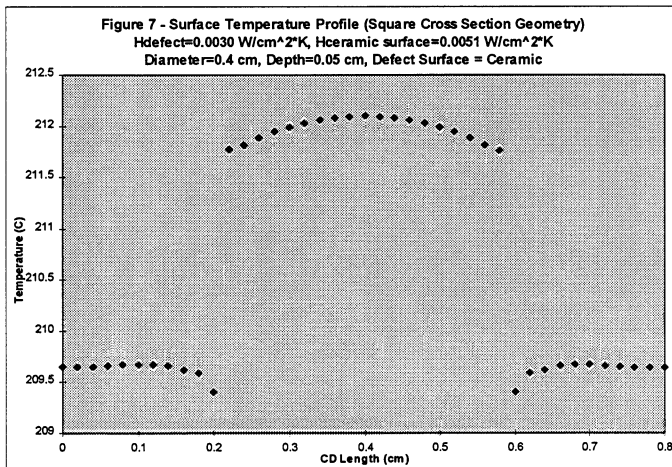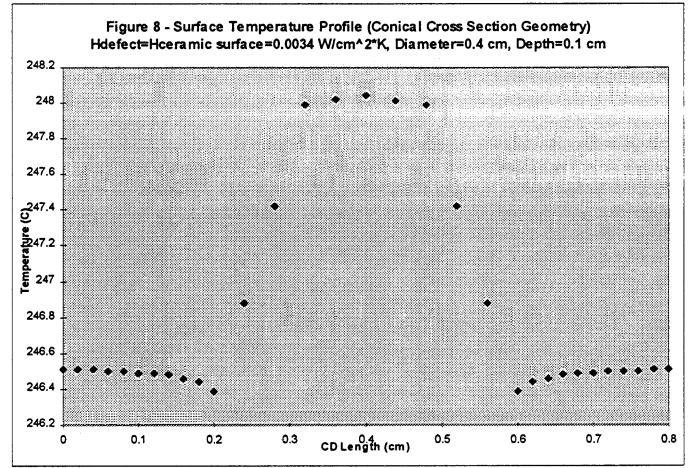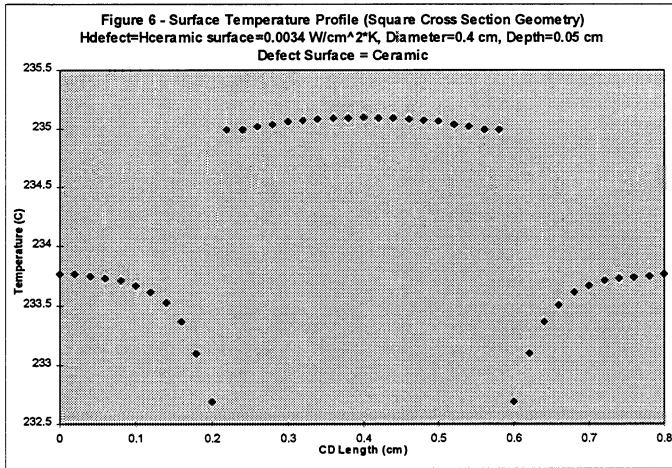

Fig. 5 MD temperature profile comparison between line and circular defects.

the grinding wheel. This created a cut not to metal, but only into the cermet coating.

On the line defects, it was observed that negative temperature differentials relative to the surface temperature were located on the tips of these lines and were outside of the defect cavity. It was also observed that these areas tended to be at the trailing edge of the defect with regard to the rotational motion of the roll and surrounding air. The AGEMA data for these areas were analyzed. It was calculated from the temperature data that the convective heat loss coefficient (H) must be 7% higher at the tips for the negative temperature differential to exist, assuming the surrounding surface and tip surface have equivalent emissivities and conduction coefficients. This suggested that the convection coefficient may be a possible explanation for the negative temperature differentials. From a surface energy balance: Qcond = Qconv + Qrad, it was determined that for the operating temperature range of the roll surface (~200°C) the convective heat losses are more than twice the radiation heat losses. Therefore, convection is a significant heat loss mode in the system.

Because convection heat loss is a more significant contributor to the system than radiation, a 2-D convection heat loss model was used to examine convection coefficients involved with the negative temperature differentials. Results from the model show that changes in the convection coefficient can produce significantly different temperature profiles (See Figures 6 and 7). The convection coefficient was varied along the coating surface and the defect interior. The effect of geometry was also shown to be significant from the model results. The geometry changes affected the convection losses of the defect (See Figures 8 and 9).

The results suggest that geometry combined with convection coefficient changes is responsible for the various temperature

6

Figure 6 - Surface Temperature Profile (Square Cross Section Geometry)
Hdefect=Hceramic surface=0.0034 W/cm^2*K, Diameter=0.4 cm, Depth=0.05 cm
Defect Surface = Ceramic

Figure 8 - Surface Temperature Profile (Conical Cross Section Geometry)
Hdefect=Hceramic surface=0.0034 W/cm^2*K, Diameter=0.4 cm, Depth=0.1 cm

Figure 7 - Surface Temperature Profile (Square Cross Section Geometry)
Hdefect=0.0030 W/cm^2*K, Hceramic surface=0.0051 W/cm^2*K
Diameter=0.4 cm, Depth=0.05 cm, Defect Surface = Ceramic

Figure 9 - Surface Temperature Profile (Conical Cross Section Geometry)
Hdefect=0.0030 W/cm^2*K, Hceramic surface=0.0051 W/cm^2*K
Diameter=0.4 cm, Depth=0.1 cm

Figs. 6 and 7 Temperature profiles created by the model simulating a square cross section geometry (a mill defect). Data produced in Fig. 7 uses a 33% larger convection coefficient on the surface than fig. 6.

Figs. 8 and 9 Temperature profiles generated by the model simulating the conical, or drill, defect geometry. Data produced in Fig. 9 uses a 33% larger convection coefficient on the outside surface than on the interior of the cavity.

profiles observed. A detailed investigation was not possible in this study.

CONCLUSIONS

The resolution at which surface defects can be detected by thermal imaging was determined. The smallest circular defect that could be detected was 2.38 mm (3/32") in diameter. The smallest detectable surface scratches (line defects) had a width of 1.59 mm (2/32"). This was slightly better than the circular defects. This was attributed to the cross-sectional geometry of the line defects, which allows a greater thermal gradient at the edge of the line defect.

Circular defects on the same horizontal axis (CMD) demonstrated similar temperature differentials between the defect and the surrounding coating surface. These differentials remained similar despite the presence of a

temperature gradient along the same axis. The temperature differentials decreased as the defects became smaller in diameter, but did not increase significantly once the exposed surface area exceeded a threshold value.

The differences between the measurements made using the AGEMA system and the physical measurements of the roll are believed to be due to edge effects. The edge effects appear to be the result of defect geometry and varying convection heat loss.

The technique of using high-speed infrared imaging to detect roll coating failures has proven to be an excellent method. The resolution achieved with this method can detect defects that could escalate into costly damages to paper rolls and press sections.

REFERENCES

1. D.I. Orloff, "Impulse Drying of Linerboard: Control of Delamination," 77th Ann. Meet. Can. Pulp and Paper Assoc., Montreal, Canada, January 1991.
2. D.I. Orloff and S.F. Sobczyniski, "Impulse Drying Pilot Press Demonstration: Ceramic Surfaces Inhibit Delamination," presented at SPCI-92, Bologna, Italy, May 19-20, 1992.
3. W.J. Lenling, M.F. Smith, and D.I. Orloff, "Thermal Coating Development for Impulse Drying," *Journal of Thermal Spray Technology*, 1993, p. 173-178.
4. H.T. Young and T.L. Chou, "Investigation of Edge Effect from the Chip-back Temperature Using IR Thermograhpic Techniques," *Journal of Materials Processing Technology*, 1995, p. 213-224.
5. M.P. Connolly, "A Review of Factors Influencing Defect Detection in Infrared Thermography: Applications to Coated Materials," *Journal of Nondestructive Evaluation*, 1991, p. 89-96.
6. K. Ogura and T. Sakagami, "A New Inspection Technique for Small Flaws and Defects Using Infrared Thermography," *ASME, Advances in Electronic Packaging*, 1992, p. 909-915.
7. M.E. McKnight and J.W. Martin, "Detection and Quantitative Characterization of Blistering and Corrosion of Coatings on Steel Using Infrared Thermography," *Journal of Coatings Technology*, 1989, p. 57-62.
8. S. Satonaka, H. Ohba, and K. Shinozaki, "Nondestructive Evaluation of Weld Defects by Infrared Thermography," *Proc. of the 14th Intl. Conf. on Offshore Mechanics and Artic Engineering-ASME*, 1995, vol. 3, p. 305-312.
9. M. Lahdeniemi, A. Ekholm, and O. Santamaki, "IR Frequency Analysis in Paper Industry," *Proc. of SPIE, Thermosense XVIII*, 1996, p. 2-4.
10. Thermovision 900 Series User's Manual, AGEMA Infrared Systems, Danderyd, Sweden, 1993.
11. F.P. Incropera and D.P. DeWitt, *Fundamentals of Heat and Mass Transfer, 3rd Edition*, John Wiley & Sons, 1990.
12. L.J. Segerlind, *Applied Finite Element Analysis, 2nd Edition*, John Wiley & Sons, 1984.

ACKNOWLEDGEMENTS